Effect of high strain rates on peak stress in a Zr-based bulk metallic glass

George Sunny,[1] Fuping Yuan,[1] Vikas Prakash,[1,a)] and John Lewandowski[2]
[1]*Department of Mechanical and Aerospace Engineering, Case Western Reserve University, Cleveland, Ohio 44106-7222, USA*
[2]*Department of Materials Science and Engineering, Case Western Reserve University, Cleveland, Ohio 44106-7222, USA*

(Received 10 April 2008; accepted 16 September 2008; published online 10 November 2008)

The mechanical behavior of $Zr_{41.25}Ti_{13.75}Cu_{12.5}Ni_{10}Be_{22.5}$ (LM-1) has been extensively characterized under quasistatic loading conditions; however, its mechanical behavior under dynamic loading conditions is currently not well understood. A Split–Hopkinson pressure bar (SHPB) and a single-stage gas gun are employed to characterize the mechanical behavior of LM-1 in the strain-rate regime of 10^2–10^5/s. The SHPB experiments are conducted with a tapered insert design to mitigate the effects of stress concentrations and preferential failure at the specimen-insert interface. The higher strain-rate plate-impact compression-and-shear experiments are conducted by impacting a thick tungsten carbide (WC) flyer plate with a sandwich sample comprising a thin bulk metallic glass specimen between two thicker WC target plates. Specimens employed in the SHPB experiments failed in the gage-section at a peak stress of approximately 1.8 GPa. Specimens in the high strain-rate plate-impact experiments exhibited a flow stress in shear of approximately 0.9 GPa, regardless of the shear strain-rate. The flow stress under the plate-impact conditions was converted to an equivalent flow stress under uniaxial compression by assuming a von Mises–like material behavior and accounting for the plane strain conditions. The results of these experiments, when compared to the previous work conducted at quasistatic loading rates, indicate that the peak stress of LM-1 is essentially strain rate independent over the strain-rate range up to 10^5/s. © *2008 American Institute of Physics*. [DOI: 10.1063/1.3009962]

I. INTRODUCTION

Metallic glasses have been of great interest because of their fully amorphous structure. Many researchers have reported a near theoretical peak strength for metallic glasses along with higher hardness compared with their crystalline counterparts.[1–8] In addition, these materials exhibit large elastic strains, corrosion resistance, and excellent processing ability.[1–3,9,10] Recent advances in the development of multicomponent metallic glass systems have allowed bulk samples of metallic glasses to be produced;[11,12] most of these are Zr-based, Fe-based, or Pd-based. These bulk metallic glass (BMG) samples have facilitated mechanical testing using conventional means.

While many experiments have been conducted on these BMGs in the quasistatic strain-rate regime (i.e., 10^{-5}–10^{-1}/s),[1–8,13–15] data on their behavior at elevated strain-rates ($>10^2$/s) have been limited,[13–18] particularly in the high strain rate ($>10^4$/s) loading regime.[19–21] Most researchers have performed experiments using the Split–Hopkinson pressure bar (SHPB) in order to investigate the behavior, first, by determining the peak stresses and temperature rise,[8,13–15,17] and then by close examination of the fracture surfaces to allow for comparison between the quasistatic and dynamic behavior.[14,18] Some of these works were performed to rationalize the reported apparent neutral[14,16,17] and/or negative strain-rate sensitivity to temperature rise[13,15] under quasistatic and dynamic loading conditions, while a recent research[18] has suggested that stress concentrations, which are an artifact of the experimental geometry employed, may be responsible for the observed negative strain-rate sensitivity. Limited work has also been conducted using plate-impact experiments to examine stress-strain behavior at higher strain-rates and also to understand the shock-induced wave structure,[20] Hugoniot elastic limit (HEL),[19,21] and spall strength.[19]

In this study, both SHPB and combined compression-and-shear plate-impact experiments are performed on $Zr_{41.25}Ti_{13.75}Cu_{12.5}Ni_{10}Be_{22.5}$ (LM-1) to determine the sensitivity of its peak stress to strain rates in the 10^2–10^5/s range. The SHPB experiments are conducted with tapered inserts previously discussed[18] to mitigate the effects of stress concentrations that have been well-documented for low strain-to-failure materials.[22–25] Strain gages are attached to selected cylindrical LM-1 specimens in order to determine accurately the strains experienced by the specimens. An ultra-high-speed camera (Imacon 200) is also employed to perform *in situ* video of the flow and fracture processes of selected specimens. The plate-impact combined-and-shear experiments are conducted using a single-stage gas gun. These experiments involve the skew impact of a thick WC flyer plate with a stationary target plate comprising a thin BMG specimen sandwiched in between a front and back WC plates. The normal and transverse components of the free-surface particle velocity histories, measured by using a multibeam VALYN™ VISAR, are used to determine the flow stress in shear at ultrahigh (e.g., $>10^5$/s) strain rates.

a)Electronic mail: vikas.prakash@case.edu.

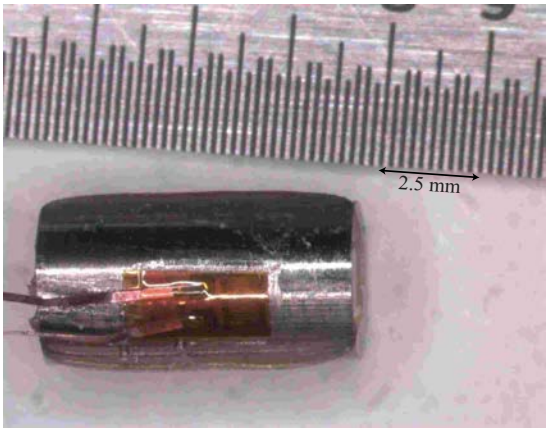

FIG. 1. (Color online) Specimen with strain gage attached prior to removal of epoxy and detachment of leads. The barreled appearance is due to the presence of epoxy around the strain gage.

II. EXPERIMENTAL PROCEDURE

The material used was LM-1 (Liquidmetal, Inc.) and was received in the form of two plates: one of dimensions $90 \times 63 \times 5$ mm^3 and one of dimensions $38 \times 38 \times 0.7$ mm^3. Both plates were verified to be fully amorphous (differential scanning calorimetry and x-ray diffractometry) by Liquidmetal and in previous works.[5–7,26,27]

A. SHPB experiments

The SHPB specimens were produced from the larger plate. The plate was electrical-discharge machined into rectangular bars, which were then centerless ground into cylindrical rods of diameter 4.0 mm. These bars were then metallographically polished using a combination of SiC-grit sandpaper and diamond paste. Right cylindrical specimens of $L/D = 1.0$ and 2.0 were then prepared using a low speed saw (Buehler, Model 11–1180) to ensure flatness and parallelism. The resulting specimens were then lapped and polished to a 6 μm finish. Strain gages (Vishay, model EA-06-031CE-350 with attached leads) are attached to selected specimens by fixing the specimens on a glass plate and applying the strain gages on the specimen with M-BOND10 high-strength epoxy. The tape is held down with weights in order to ensure even tension in the tape and even pressure on the strain gage during the 18 h curing process. After curing, the excess epoxy is removed and the lead wires are detached from the specimen to prevent any shorting of the wires during the experiment. The resulting setup (Fig. 1) is then connected to a Wheatstone bridge and is in turn connected to a differential amplifier (Tektronix 5A22N) to be recorded by a high-bandwidth oscilloscope (Tektronix 680). Stress concentrations were mitigated through the use of rounded maraging steel inserts, while molybdenum disulfide grease (Sta-lube) was utilized between the inserts and the specimen to provide low friction at the specimen-insert interface.

The SHPB (discussed in detail elsewhere[24]) at Case Western Reserve University consists of a pressurized air gas gun and three 19.05 mm diameter maraging steel (Vascomax 350) bars—a 0.2 m long striker bar, a 1.6 m long incident bar, and a 1.5 m long transmitted bar. Semiconductor strain

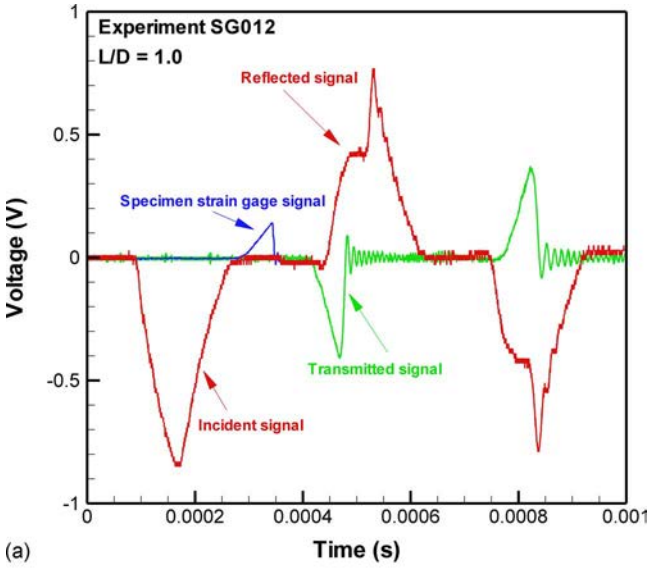

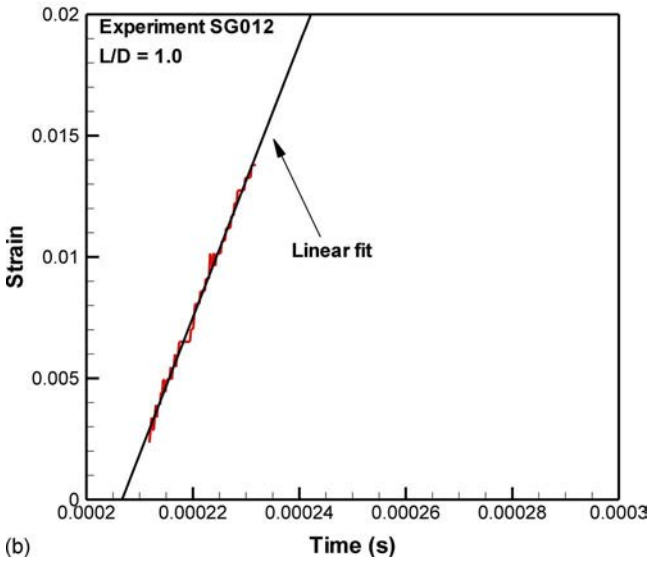

FIG. 2. (Color online) (a) Strain history signals from the strain gages mounted on the incident bar, transmitted bar, and specimen. (b) Specimen strain vs time profile determined from (a) showing constant strain-rate conditions.

gages (Vishay BLH, model SR-4) are attached diametrically opposite each other on the incident and transmitted bars to eliminate any effects of bending on the strain history of each bar. All four strain gages are attached to Wheatstone bridges, which are in turn connected to two differential amplifiers (Tektronix 5A22N). The strain histories for each of the bars are recorded by a high-bandwidth oscilloscope (Tektronix 680). The recorded signals from the incident and transmitted bars were converted to the appropriate strain-rate, strain, and stress histories of the specimen via accepted procedures. The signals recorded by the specimen were converted to stresses by assuming that the specimen is linearly elastic to failure, an assumption that is reasonable based on past results at quasistatic[5–8] and dynamic strain rates.[16,17]

The limited strain-to-failure of LM-1 necessitates the use of pulse shaping;[24,28] therefore, copper pulse shapers were utilized to control the shape and rise time of the incident pulse and thus promote equilibrium conditions in the speci-

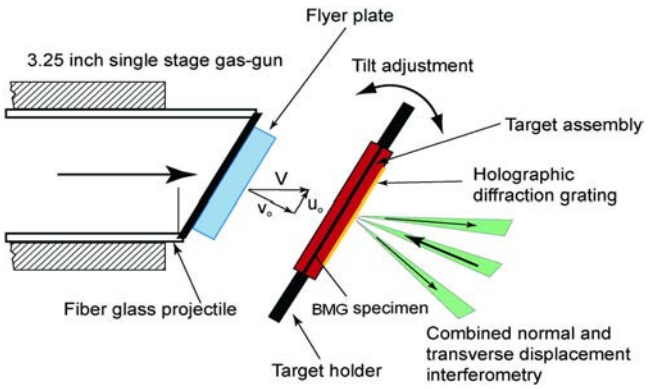

FIG. 3. (Color online) Schematic of the plate-impact pressure-shear experiment.

men. The pulse shapers used were ~7–8 mm on a side with a thickness of 0.6–0.7 mm. Strain gages on the specimen were used to ensure that the specimen is deforming under constant strain-rate conditions. Figure 2 shows an example of a typical strain versus time signal from the specimen strain gage. Based on the linear strain versus time curve, it is apparent that the specimen is under a constant strain rate starting at a strain of approximately 0.3%.

B. Plate-impact experiments

Thin square plates of dimensions $38\times38\times0.7$ mm^3 were utilized for the plate-impact experiments. These plates were lapped and polished to ensure a 5 μm surface finish; the resulting thickness of the plates was approximately 0.6 mm.

C. Experimental configuration

The plate-impact experiments were conducted using the 82.5 mm bore single-stage gas gun in the Department of Mechanical and Aerospace Engineering at Case Western Reserve University. The high strain-rate plate-impact pressure-shear experiment involves the impact of a thick WC flyer plate mounted on a projectile with a stationary target. The target consists of the thin BMG plate sandwiched in between

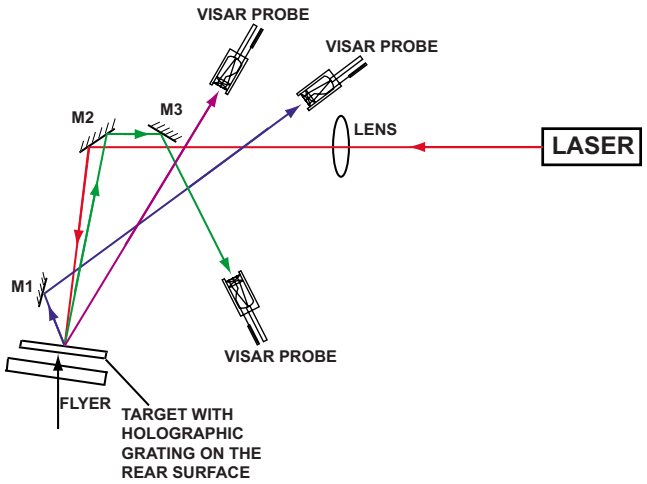

FIG. 4. (Color online) Schematic of the combined normal and transverse velocity interferometer.

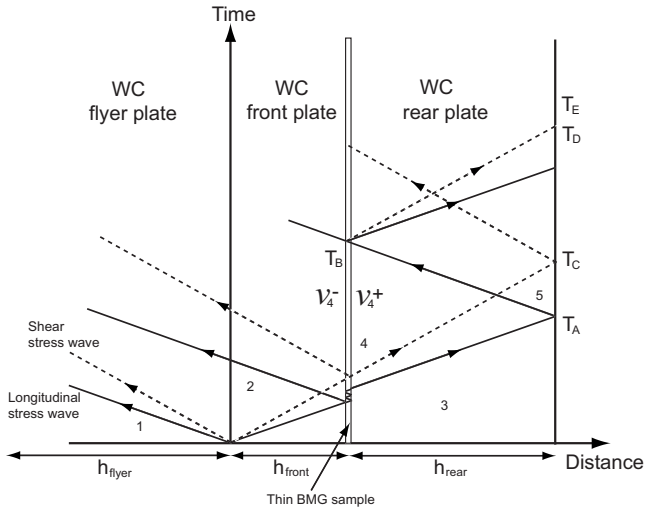

FIG. 5. Wave propagation in the flyer and the target plates (*t-X* diagram) for a typical plate-impact pressure-shear experiment.

a front and a back WC plate. The corresponding experimental configuration is shown in Fig. 3. The rear end of the projectile has a sealing O-ring and a Teflon key that slides in a key way inside the gun barrel to prevent any rotation of the projectile. In order to reduce the possibility of air cushion between the flyer and target plates, impact takes place in a target chamber that has been evacuated to 50 μm of Hg prior to impact. To ensure the generation of plane waves with wave fronts sufficiently parallel to the impact face, the flyer and the target plates are ground and lapped flat, and they are aligned to be parallel to within 2×10^{-5} rad using an optical alignment scheme developed by Kim *et al.*[29] The actual tilt between the two plates is measured by recording the times at which four isolated and voltage-biased pins, which are flushed with the surface of the target plate, are shorted to ground. A laser-based optical system, utilizing a helium-neon 5 mW laser (UNIPHASE 1125p) and a high frequency photodiode, was used to measure the velocity of the projectile. Impact takes place at an angle θ relative to the direction of approach. Upon impact, both longitudinal and shear waves are generated within the flyer and target plate, leading to pressure-shear loading of the sandwiched specimen. In all tests the projectile velocity and the skew angle are controlled such that all WC plates (the flyer, the front, and back target plates) remain elastic during impact. Other details regarding the design, execution, and data analysis of the experiments can be found elsewhere.[30]

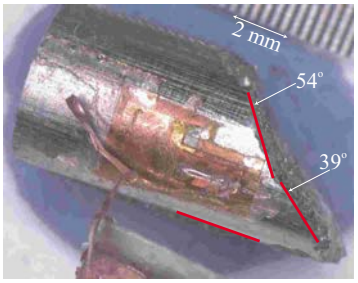

FIG. 6. (Color online) Optical microscopy of as-cast specimen, $L/D=2.0$, after testing, showing that the strain gage is still adhered to the sample surface.

TABLE I. List of SHPB experiments conducted on LM-1 in which specimen failure occurred before strain gage separation from the specimen.

Experiment	Striker velocity (m/s)	Peak strain	Peak stress (MPa)	Specimen failed?	Strain gage separated?
SG004	8.8	1.89%	1810	Yes	No
SG005	10.3	1.83%	1750	Yes	No
SG008	10.2	1.97%	1890	Yes	No
SG011	8.5	1.95%	1870	Yes	No
SG012	9.0	1.70%	1630	Yes	No
SG013	8.8	2.2%	2000	Yes	No

[a]Assumed to yield prior to failure.

A laser interferometer based on the multibeam VALYN™ VISAR is used to measure the combined normal and transverse particle velocities at the free surface of the target plate. The schematic of the light path of the laser interferometer is shown in Fig. 4. Three VALYN™ VISAR fiber-optic channels are simultaneously employed to obtain the normal and transverse components of the free surface of the target plate by collecting the 0 and ± 1 order diffraction beams from a holographic grating deposited on the rear surface of the target plate. In the present experiments a holographic diffraction grating with a pitch of 1200 lines/mm is utilized.

Following Chhabildas *et al.*,[31] the longitudinal and the transverse components of the free-surface particle velocity, i.e., $U(t)$ and $V(t)$, can be expressed in terms of the measured particle velocities along the $\pm$ beams, i.e., $V^{\pm}(t)$, and the diffraction angle θ_{VISAR} as

$$U(t) = \frac{V^{+}(t) + V^{-}(t)}{(1 + \cos\ \theta_{\mathrm{VISAR}})}, \tag{1}$$

$$V(t) = \frac{V^{+}(t) - V^{-}(t)}{\sin\ \theta_{\mathrm{VISAR}}}. \tag{2}$$

The time-distance diagram showing the propagation of both longitudinal and transverse waves in the flyer and the target plated is shown in Fig. 5. Since the flyer, the front, and rear target plates are designed to remain elastic during impact, the normal stress and the particle velocity in the BMG specimen (state 4) can be obtained by using characteristic equations in terms of the measured normal component of the free surface particle velocity $u_{\mathrm{fs}}(t)$ and the longitudinal impedance of the WC target plates ρC_L as

$$\sigma_4 = -\frac{1}{2}(\rho C_L) u_{\mathrm{fs}}(t). \tag{3}$$

In a typical plate-impact combined compression-and-shear experiment, by the time the shear is imposed on the specimen, a nominally homogeneous normal stress state is present. Under these conditions, the rate of deformation in the thin BMG specimen can be expressed as a simple-shear deformation rate, with shearing in the 1-2 plane. The shear stress within the specimen can be expressed as

$$\tau_4 = -\tfrac{1}{2}(\rho C_S) v_{\mathrm{fs}}(t). \tag{4}$$

In Eq. (4), $v_{fs}(t)$ is the measured transverse component of the free surface particle velocity, while ρC_S is the transverse impedance of the WC target plates. The nominal shear rate in the specimen can be expressed as

$$\dot{\gamma}(t) = \frac{v_4^{-} - v_4^{+}(t)}{h(t)} = \frac{V_0 \sin\ \theta - v_{\mathrm{fs}}(t)}{h(t)}, \tag{5}$$

where $h(t)$ is the thickness of the thin BMG specimen. Using Eq. (5), the shear strain $\gamma(t)$ in the specimen can be obtained by integrating the shear strain rate over the total time duration, i.e.,

$$\gamma(t) = \int_0^t \dot{\gamma} dt. \tag{6}$$

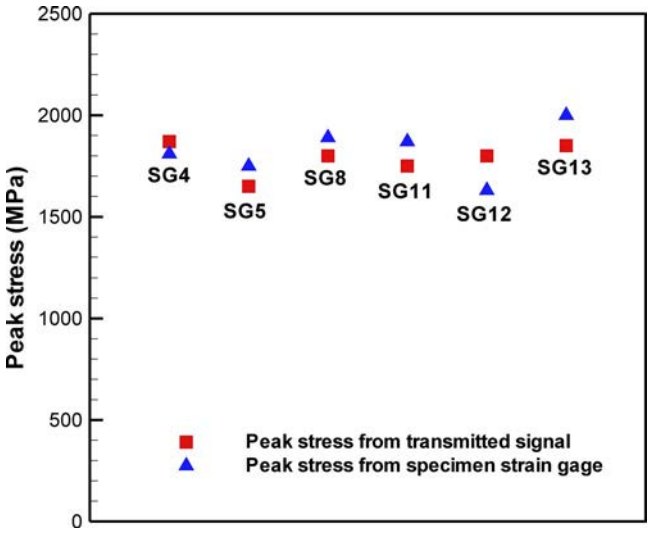

FIG. 7. (Color online) Peak stresses as determined from transmitted and specimen strain gage signals.

III. EXPERIMENTAL RESULTS AND DISCUSSION

A. SHPB experiments

Table I summarizes the key parameters—striker bar velocity, peak strain, and peak stress—for the six successful experiments conducted. Additional experiments were conducted but were not included either because of premature

TABLE II. List of pressure-shear plate-impact experiments performed.

Experiment	BMG (mm)	Flyer WC (mm)	Front WC target plate (mm)	Rear WC target plate (mm)	Impact velocity (m/s)	Skew angle (°)
1	0.58	6.59	3.65	4.83	189.9	22
2	0.60	6.59	3.60	4.83	178.4	15
3	0.44	6.55	3.61	4.81	143.4	22

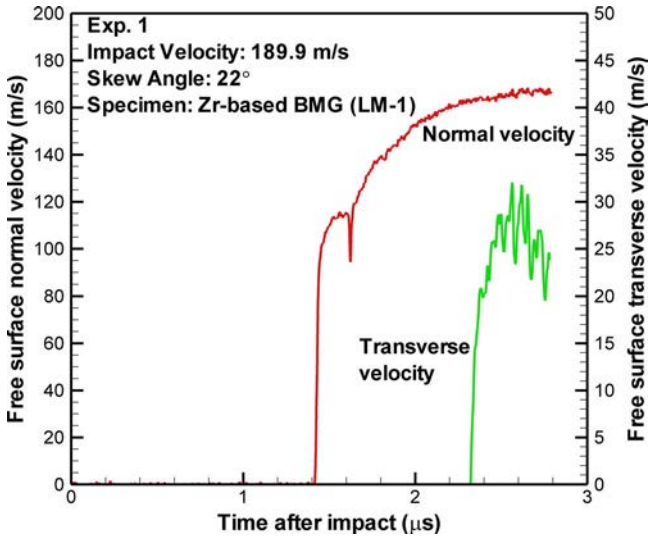

FIG. 8. (Color online) Longitudinal and transverse free surface velocities for experiment 1.

separation of the specimen strain gage from the specimen surface, which would underestimate the peak strains and stresses experienced by the specimen, or because the specimen did not fail. In addition, Fig. 6 shows one such specimen after the experiment is conducted; the strain gage is clearly still present on the specimen, and the specimen appears to exhibit two fracture angles. High-speed video (shown elsewhere[18]) clearly shows that the failure is occurring in the gage section of the specimen and not at the specimen-insert interface.

Comparison of the stress-strain data from the SHPB experiments suggests that the strain-rate sensitivity of BMG is negligible, as seen from Fig. 7; the experimental errors present have been determined to be approximately 8%–10%, in accordance with previous peak stress measurements using the SHPB on other low strain-to-failure materials. For a given strain-rate and varying L/D (such as experiments SG 4 and SG 11, both of which exhibit a strain-rate of approximately 350/s), the effect of the L/D ratio on the peak stress of LM-1 can also be considered to be negligible. The peak stress seems to be similar for all six experiments.

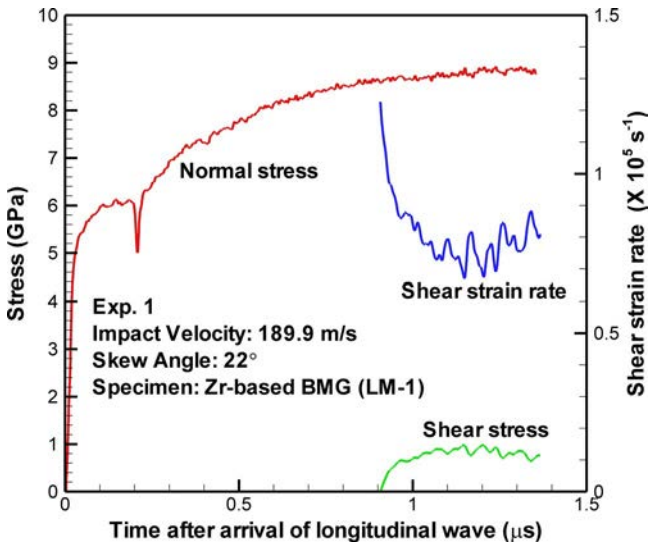

FIG. 9. (Color online) History of normal stress, the shear stress, and the shear strain rate in the specimen for experiment 1.

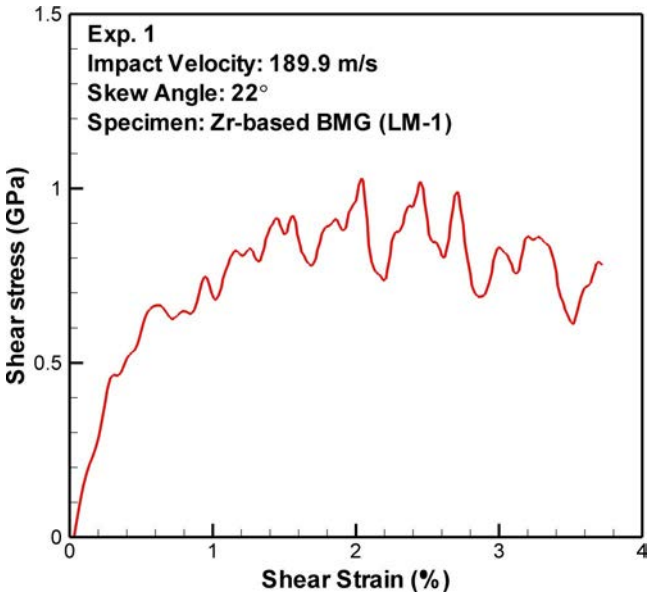

FIG. 10. (Color online) Dynamic shear stress vs shear strain for experiment 1.

B. Plate-impact experiments

The key parameters—shot number, thickness of BMG specimen, thickness of WC flyer plate, thickness of front and rear plates, impact velocity, and skew angle—for the three experiments conducted in this series are shown in Table II.

Figures 8–10 summarize the results for experiment 1. Figure 8 shows the history of the longitudinal and transverse components of the free surface particle velocities measured using the multibeam VALYN™ VISAR. Figure 9 shows the corresponding time history of the normal stress, shear stress, and the shear strain rate in the specimen, obtained by using the Eqs. (3) and (4). Upon arrival of the longitudinal wave at the specimen plane, the normal stress in the specimen builds up to a level of 8.85 GPa. Based on the longitudinal impedance of the WC front and rear target plates and the BMG specimen, near-equilibrium (homogeneous) stress conditions are expected to be achieved in the specimen in about 500 ns (corresponding to four reverberations of the longitudinal wave in the specimen). The details of the normal stress buildup can be seen as a sequence of steps in the normal stress profile before it reaches a plateau. Since the speed of the transverse wave in the front target plate is lower than the longitudinal wave speed, the shear wave arrives at the specimen after approximately 0.9 μs of the arrival of the longitudinal pulse. Upon arrival of the shear wave at the specimen plane the shear stress rings up in the thin sandwiched specimen, as the specimen undergoes a combined compression-and-shear deformation. Based on the transverse impedance of the WC target plates and the BMG specimen, it takes about 250 ns for a state of simple shearing to develop to a level of ~0.92 GPa in shear within the BMG specimen. The shearing rate during this pressure-shear deformation is ap-

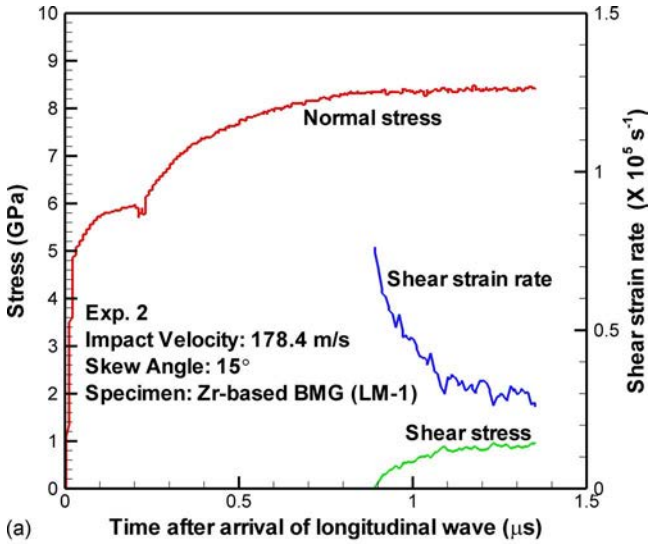

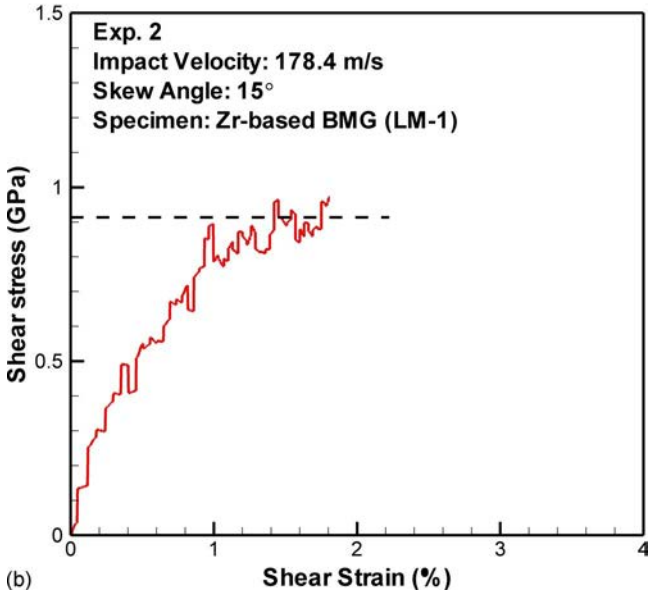

FIG. 11. (Color online) History of (a) normal stress, shear stress, and shear strain-rate for experiment 2 and (b) shear stress vs shear strain in the specimen for experiment 2.

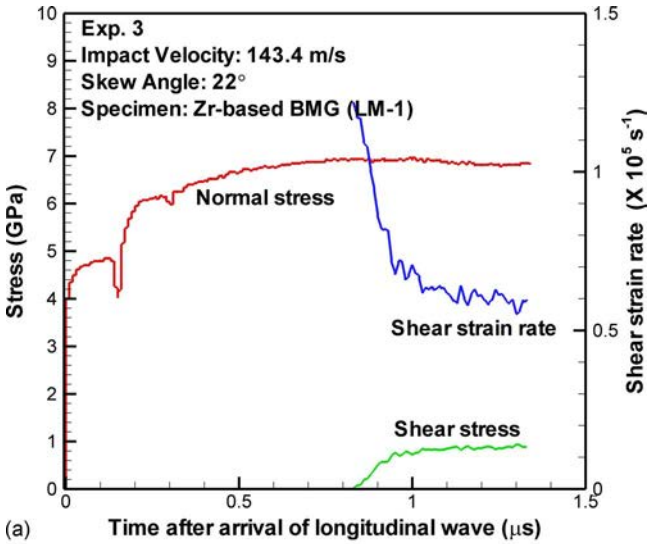

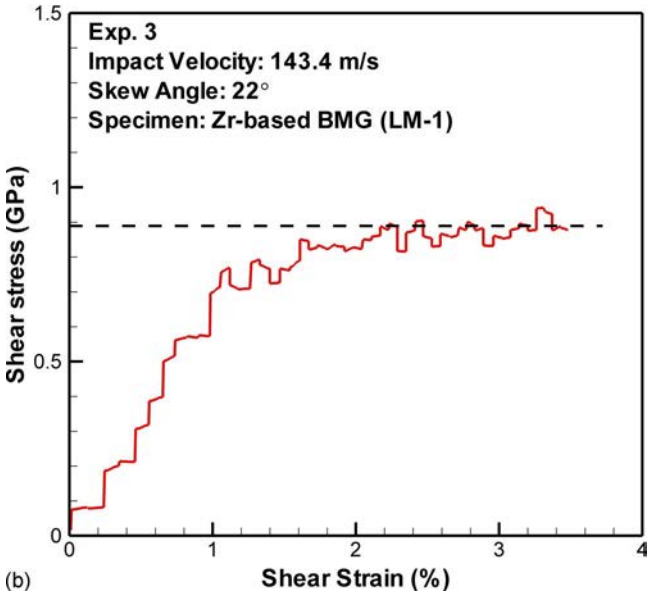

FIG. 12. (Color online) History of (a) normal stress, shear stress, and shear strain-rate for experiment 3 and (b) shear stress vs shear strain in the specimen for experiment 3.

proximately 0.75×10^5 s^{-1}. Figure 10 shows the shear stress versus the accumulated shear strain within the specimen. It is important to note that by the time the shear wave arrives at the specimen plane a state of essentially homogeneous normal stress is present in the BMG specimen.

The results of experiment 2 are shown in Fig. 11. Experiment 2 was conducted with a smaller skew angle (15°) compared with 22° that was employed in experiment 1. As a result, the shearing rate in the specimen is much smaller ($\sim0.32\times10^5$ s^{-1}). Figure 11(a) shows the history of normal stress, the shear stress, and the shear strain-rate within the specimen. Upon arrival of the longitudinal wave at the specimen plane, the normal stress builds up to a level of approximately 8.36 GPa. The transverse wave arrives at the specimen after approximately 0.9 μs of the arrival of the longitudinal pulse. At the arrival of the shear wave the BMG specimen undergoes simple shearing deformation. Figure 11(b) shows the shear stress (σ_{12}) versus shear strain re-

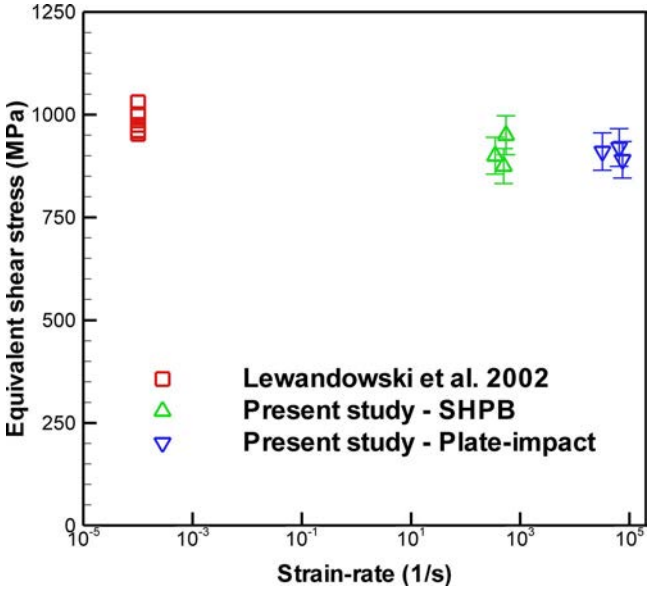

FIG. 13. (Color online) Effect of strain rate on equivalent peak shear stress exhibited by LM-1 for the strain rates ranging from 10^{-4} to 10^5/s.

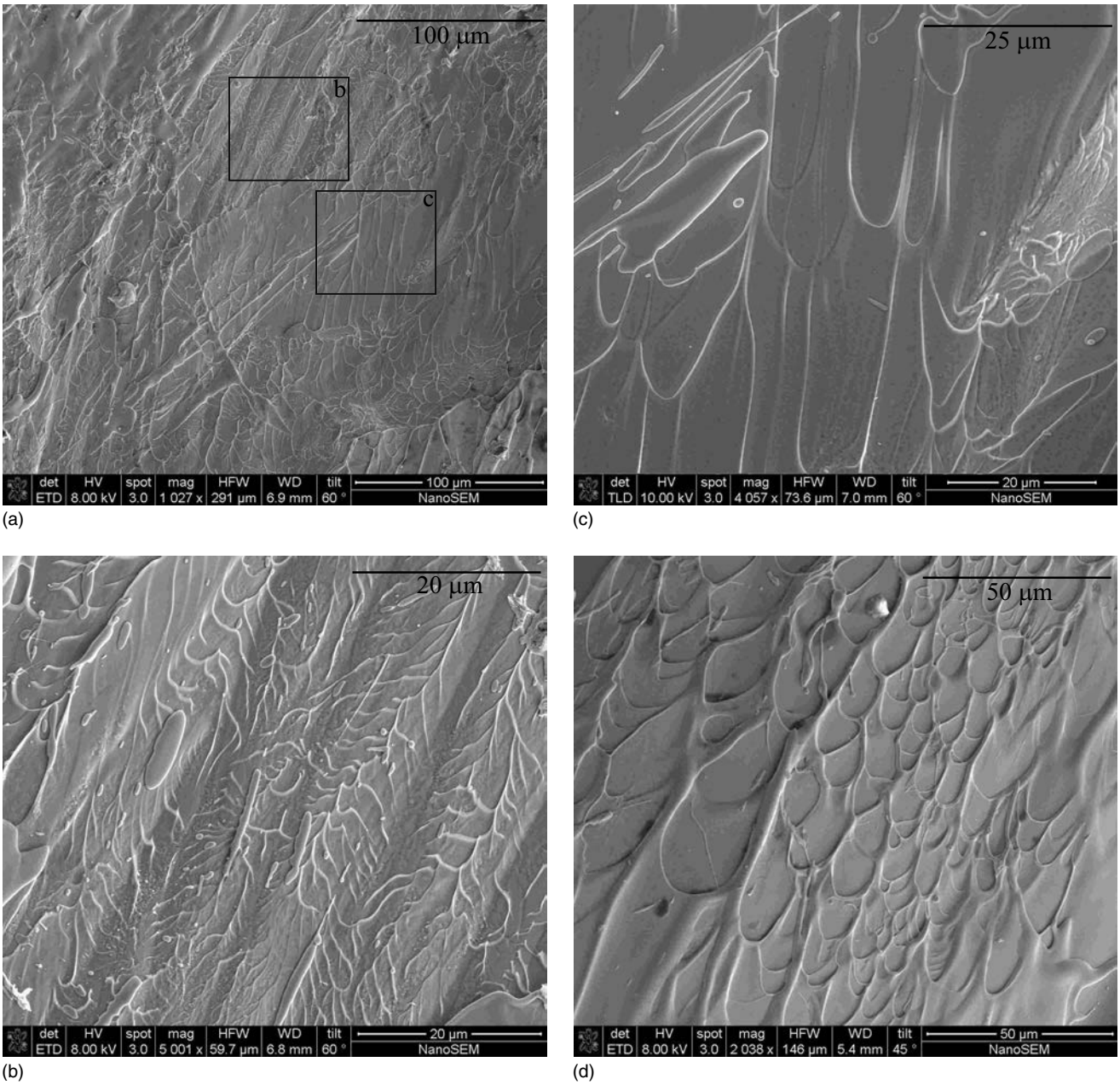

FIG. 14. (a) SEM images of a specimen tested under dynamic conditions ($L/D=2.0$, strain rate of 350 /s). Images show (b) veining patterns in the low-viscosity regions as well as (c) the presence of elongated cusps, while (d) other regions reveal the presence of more equiaxed cusps.

sponse of the sandwiched BMG specimen. As in experiment 1, the shear strength of the BMG specimen is approximately 0.9 GPa.

The results for experiment 3 are shown in Fig. 12. Experiment 3 was designed to be conducted at the same skew angle as experiment 1 (22°) but at a lower impact velocity (143 m/s). As a result, the normal stress level was only 6.92 GPa, much lower than that obtained in experiments 1 and 2. Figure 12(a) shows the history of the normal stress, shear stress, and shear strain rate within the specimen. Upon the arrival of the longitudinal wave at the specimen plane, the normal stress in the specimen builds up to a level of approximately 6.92 GPa in a sequence of steps before it reaches a plateau. Figure 12(b) shows the shear stress (σ_{12}) versus shear strain response of the specimen. The shear strength of the BMG specimen becomes steady at around 2% shear strain and is estimated to be 0.89 GPa. The corresponding shear strain rate in the specimen is 0.65×10^{5} s^{-1}.

Because the SHPB experiments measure compressive peak stress under plane stress conditions and the gas gun experiments measure the shear stress under plane strain conditions, it is necessary to convert the shear stresses measured into an equivalent compressive stress. While different yielding criteria have been proposed for LM-1,[5,8,32] the most typical one is a Mohr–Coulomb relationship of the form

$$\tau = \tau_c - k\sigma,$$

$$k = \cot(\alpha), \tag{7}$$

where τ and σ are the shear and normal stresses acting on a surface, τ_c is the maximum shear stress exhibited in torsion, and the constant k is the normal stress dependency param-

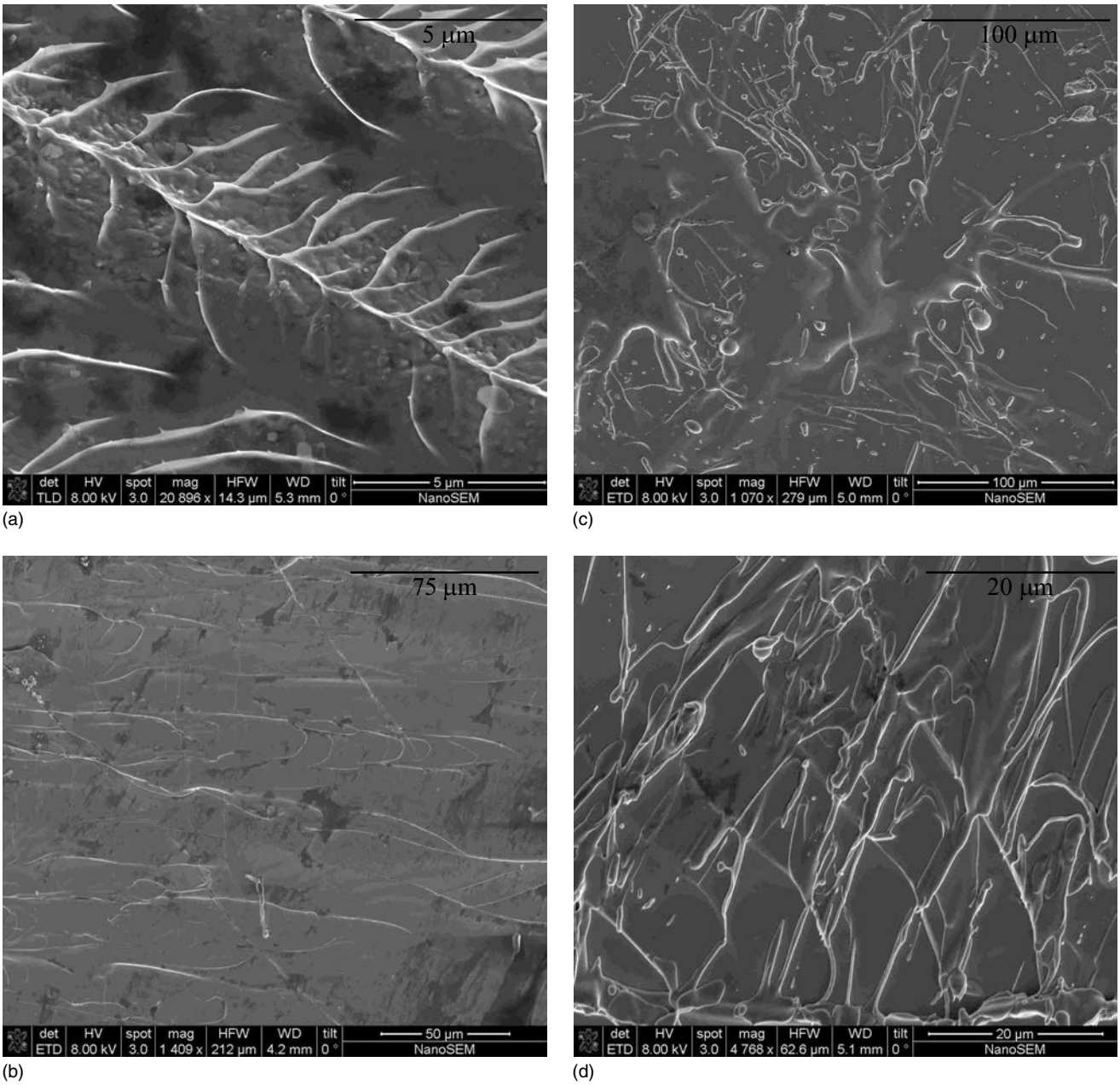

FIG. 15. SEM images of a specimen tested under quasistatic conditions ($L/D=1.9$, strain rate of $10^{-4}/s$). Images show (a) veining patterns and (b) elongated cusps, similar to Figs. 14(b) and 14(c), along with [(c) and (d)] smeared regions due to deformation and viscous flow.

eter, which can be related to the fracture angle of compression α, and when $k=0$, this becomes a von Mises–like failure criterion. The small values of k (0.02–0.06) previously found for LM-1, therefore, justify the use of the von Mises failure criterion to determine the equivalent uniaxial normal stress. Converting the SHPB normal stresses into equivalent shear stresses gives a peak stress of 0.9–1.0 GPa, as shown in Fig. 13. In addition, the Young's modulus for LM-1 under these shock-loading conditions is approximately 100 GPa, a value in close agreement with the quasistatic elastic modulus of LM-1. The similar values of Young's modulus in both the quasistatic and shock-loading conditions justify the assumed value of Young's modulus (96 GPa) used in the SHPB experiments discussed earlier.

As noted before, there have been different observations on the strain-rate sensitivity of different BMGs. While LM-1 appears to exhibit negligible strain-rate sensitivity between $10^{-4}/s$ and $10^{5}/s$, other BMGs have been seen to exhibit negative strain-rate sensitivities.[13,15,33] One factor that may have an impact in the observed negative strain-rate sensitivity is the presence of stress concentrations in the specimen during the SHPB experiment. Previous experiments[18,34] showed that the presence of stress concentrations can elevate the normal and shear stresses at the specimen-bar interface, thereby creating a nonuniform state of stress in the specimens. Since the detrimental effects of stress concentration are expected to amplify and lead to premature failure in the specimens as the impact velocity is increased in an attempt to increase the specimen strain rates, it is possible that the measure of the previously observed negative strain-rate sensitivities may contain artifacts due to the standard experi-

mental configuration used and the stress concentrations present.

In an attempt to understand better the observed neutral strain-rate sensitivity in LM-1, scanning electron microscopy was also performed on the fracture surfaces of specimens tested under quasistatic and dynamic uniaxial compression using a field emission scanning electron microscope (SEM). (In order to compare fracture surfaces of shock-loaded LM-1 to the other specimens shock recovery plate impact experiments need to be performed.) The SEM stage was tilted sufficiently to ensure that the beam and the fracture surface were nearly orthogonal to each other. Figure 14 shows representative images of the fracture surface. In particular, Fig. 14(a) shows that several features that have been previously discussed, such as "smearing" that occurs during and after failure. Figures 14(b) and 14(c) reveal the presence of extensive veining patterns and elongated cusps, respectively, formed during the highly localized inelastic flow of low viscosity BMG material. In addition, there are also more equiaxed cusps present on the fracture surface, as shown in Fig. 14(d). In comparison, representative images of the fracture surfaces from a specimen tested under quasistatic compression are shown in Fig. 15. Figure 15(a) shows regions of veining, such as those in Fig. 14(b). The low viscosity flow also reveals the presence of elongated cusps due to viscous flow, as shown in Fig. 15(b), as well as smeared regions along the fracture surface, as shown in Figs. 15(c) and 15(d). The largely similar fracture surface features (veining, low-viscosity flow, and smearing) provide further evidence of the observed insensitivity of LM-1 to strain-rate.

IV. SUMMARY

Both SHPB and pressure-shear plate-impact gas-gun experiments have been performed on LM-1, a Zr-based BMG, in order to characterize the mechanical behavior at strain-rates up to $10^5/\mathrm{s}$. The SHPB experiments were carried out with a tapered insert design in order to mitigate stress concentration effects. A peak stress of approximately 1.8 GPa was exhibited by the specimens under these conditions. From the pressure-shear plate-impact experiments a flow stress in shear of approximately 0.9 GPa is obtained, regardless of material strain rate. Comparison of the present peak stresses to those obtained on LM-1 under quasistatic conditions reveals that LM-1 appears to be strain-rate independent for strain rates between 10^{-4} and $10^5/\mathrm{s}$.

ACKNOWLEDGMENTS

The authors acknowledge Liquidmetal, Inc. for producing and supplying some of the BMG plates used in the experiments, along with Mike Bifano for the SEM images in the paper. Partial funding for this work is provided by a Case Prime Fellowship (GS, FY) (Grant Nos. ONE-N00014-03-1-0205 and DARPA-ARO-DAAD19-01-0525). Funding for the high-speed camera was provided by NSF MRI, Grant No. CMS 0079458.

[1]A. Inoue, T. Zhang, and T. Masumoto, Mater. Trans., JIM **31**, 425 (1990).
[2]A. Inoue, Y. Nakamura, N. Nishiyama, and T. Masumoto, Mater. Trans., JIM **33**, 937 (1992).
[3]T. Zhang, A. Inoue, and T. Masumoto, Mater. Trans., JIM **32**, 1005 (1991).
[4]X. J. Gu, S. J. Poon, and G. J. Shiflet, J. Mater. Res. **22**, 344 (2007).
[5]J. J. Lewandowski and P. Lowhaphandu, Philos. Mag. A **82**, 3427 (2002).
[6]P. Lowhaphandu, L. A. Ludrosky, S. L. Montgomery, and J. J. Lewandowski, Intermetallics **8**, 487 (2000).
[7]P. Lowhaphandu, S. L. Montgomery, and J. J. Lewandowski, Scr. Mater. **41**, 19 (1999).
[8]H. A. Bruck, T. Christman, A. J. Rosakis, and W. L. Johnson, Scr. Metall. Mater. **30**, 429 (1994).
[9]H. X. Li, K. B. Kim, and S. Yi, Scr. Mater. **56**, 1035 (2007).
[10]A. Peker and W. L. Johnson, Appl. Phys. Lett. **63**, 2342 (1993).
[11]A. Inoue, *Bulk Amorphous Alloys: Preparation and Fundamental Characteristics*, Vol. 4 (Trans Tech Publications Inc., Stafa-Zurich, Switzerland, 1998).
[12]W. L. Johnson, Mater. Sci. Forum **225–227**, 35 (1996).
[13]T. C. Hufnagel, T. Jiao, L. Q. Xing, and K. T. Ramesh, J. Mater. Res. **17**, 1441 (2002).
[14]G. Subhash, R. J. Dowding, and L. J. Kecskes, Mater. Sci. Eng., A **334**, 33 (2002).
[15]G. Subhash, H. Zhang, and H. Li, in *Proceedings of the International Conference of Mechanical Behavior of Materials (ICM-9)*, edited by S. R. Bodner, D. Rittel, and D. Sherman (Kenes International, Geneva, Switzerland, 2003), p. 1A5.
[16]H. A. Bruck, A. J. Rosakis, and W. L. Johnson, J. Mater. Res. **11**, 503 (1996).
[17]J. Lu, G. Ravichandran, and W. L. Johnson, Acta Mater. **51**, 3429 (2003).
[18]G. Sunny, V. Prakash, and J. J. Lewandowski, J. Mater. Res. **22**, 389 (2007).
[19]F. Yuan, V. Prakash, and J. J. Lewandowski, J. Mater. Res. **22**, 402 (2007).
[20]M. Martin, T. Sekine, T. Kobayashi, L. Kecskes, and N. N. Thadhani, Metall. Mater. Trans. A **38**, 2689 (2007).
[21]S. Zhuang, J. Lu, and G. Ravichandran, Appl. Phys. Lett. **80**, 4522 (2002).
[22]W. R. Blumenthal and G. T. Gray III, in *Proceedings of the American Physical Society Topical Conference*, Vol. 2, edited by S. C. Schmidt, J. N. Johnson, and L. W. Davidson (Elsevier, Amsterdam, 1989), pp. 393–396.
[23]W. R. Blumenthal and G. T. Gray III, in *Fourth International Conference on the Mechanical Properties of Materials at High Rates of Strain*, Vol. 102 (Institute of Physics, Oxford, UK, 1989), pp. 363–370.
[24]G. T. Gray, in *American Society for Materials Handbook* (American Society for Materials International, Materials Park, OH, 2000), Vol. 8, pp. 462–476.
[25]C. A. Tracy, J. Test. Eval. **15**, 14 (1987).
[26]J. J. Lewandowski, Mater. Trans. **42**, 633 (2001).
[27]P. Lowhaphandu and J. J. Lewandowski, Scr. Mater. **38**, 1811 (1998).
[28]D. Frew, M. Forrestal, and W. Chen, Exp. Mech. **42**, 93 (2002).
[29]K. S. Kim, R. J. Clifton, and P. Kumar, J. Appl. Phys. **48**, 4132 (1977).
[30]V. Prakash, Exp. Mech. **35**, 329 (1995).
[31]L. C. Chhabildas, H. J. Sutherland, and J. R. Asay, J. Appl. Phys. **50**, 5196 (1979).
[32]Z. F. Zhang, G. He, J. Eckert, and L. Schultz, Phys. Rev. Lett. **91**, 045505 (2003).
[33]H. Li, G. Subhash, X.-L. Gao, L. J. Kecskes, and R. J. Dowding, Scr. Mater. **49**, 1087 (2003).
[34]G. Sunny, F. Yuan, V. Prakash, and J. J. Lewandowski, "Design of inserts for split-Hopkinson pressure bar testing of low strain-to-failure materials," Exp. Mech. (in press).